A novel TNFRSF1A mutation associated with TNF-receptor-associated periodic syndrome and its metabolic signature

Joachim D. Steiner[1,2], Andrea Annibal[2], Raymond Laboy[2], Marie Braumann[1], Heike Göbel[3], Valentin Laasch[2], Roman-Ulrich Müller[1,4], Martin R. Späth[1], Adam Antebi[2,4] and Torsten Kubacki[1*]

1 Department II of Internal Medicine and Center for Molecular Medicine Cologne, University of Cologne, Faculty of Medicine and University Hospital Cologne, Cologne, Germany

2 Max Planck Institute for Biology of Ageing, Cologne, Germany

3 Institute of Pathology, University Hospital of Cologne, Kerpener Str. 37, 50937 Cologne, Germany.

4 Cologne Excellence Cluster on Cellular Stress Responses in Aging-Associated Diseases (CECAD), University of Cologne, Cologne, Germany.

* Corresponding author
Torsten Kubacki
University Hospital of Cologne, Kerpener Str. 37, 50937 Cologne, Germany.
E-Mail: torsten.kubacki@uk-koeln.de
ORCID ID: 0000-0001-7723-9659

Abstract

Objective:

We describe a family with a novel mutation in the TNF Receptor Superfamily Member 1A gene (TNFRSF1A) causing tumour necrosis factor receptor-associated periodic syndrome (TRAPS) with renal AA-amyloidosis.

Methods:

Case series of affected family members. We further investigated the plasma metabolome of these patients in comparison to healthy controls using mass spectrometry.

Results:

In all symptomatic family members, we detected the previously undescribed variant c.332A>G (p.Q111R) in the TNFRSF1A gene. Canakinumab proved an effective treatment option leading to remission in all treated patients. One patient with suspected renal amyloidosis showed near normalisation of proteinuria under treatment. Analysis of the metabolome revealed 31 metabolic compounds to be upregulated and 35 compounds to be downregulated compared to healthy controls. The most dysregulated metabolites belonged to pathways identified as arginine biosynthesis, phenylalanine, tyrosine & tryptophan biosynthesis and cysteine & methionine metabolism. Interestingly, the metabolic changes observed in all three TRAPS patients seemed independent of treatment with canakinumab and subsequent remission.

Conclusion:

We present a novel mutation in the TNFRSF1A gene associated with amyloidosis. Canakinumab is an effective treatment for individuals with this new likely pathogenic variant. Alterations in the metabolome were most prominent in the pathways related to arginine biosynthesis, tryptophan metabolism and metabolism of cysteine & methionine and seemed to be unaffected by treatment with canakinumab. Further investigation is needed to determine the role of these metabolomic changes in the pathophysiology of TRAPS.

Graphical Abstract

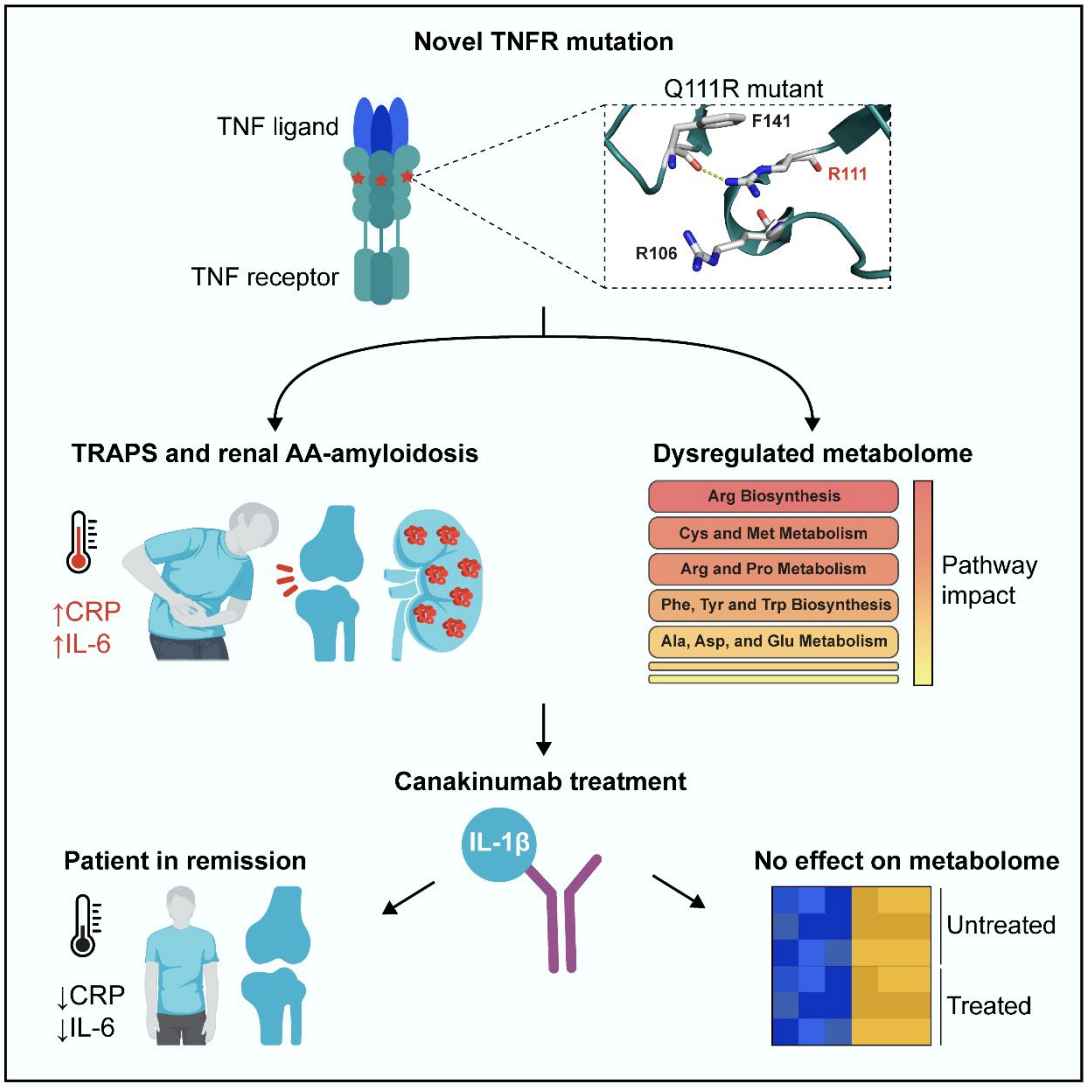

Keywords: TRAPS, Amyloidosis, Canakinumab, Metabolomics, Kidney, Kynurenine, Tryptophan, Methionine, Choline

Key messages:

- *c.332A>G (p.Q111R) is a novel pathological mutation within the TNFRSF1A-gene that causes AA-amyloidosis.*
- *Early renal amyloidosis is potentially reversible upon adequate inflammation control with canakinumab.*
- *TRAPS patients show dysregulated plasma-metabolome with marked changes in arginine, tryptophan and methionine metabolism regardless of disease activity.*

Introduction

Tumour necrosis factor receptor-associated periodic syndrome (TRAPS) is an autosomal dominantly inherited periodic fever syndrome. Heterozygous pathogenic variants in the TNF receptor superfamily member 1A (TNFRSF1A) gene cause TRAPS, which leads to dysregulation of the innate immune system and subsequent systemic inflammation(1). It is clinically characterised by prolonged episodes of fever, arthralgia, myalgia, abdominal pain and erythematous rash(2). As a rare disease, the prevalence is estimated to be around one case per million people(3, 4).

Here we report a new mutation in the TNFRSF1A gene in a Caucasian family, which is associated with TRAPS and AA amyloidosis. We also evaluate its response to treatment with the IL-1β inhibitor canakinumab. Pathologic variants in the TNFRSF1A gene disrupt the folding of the protein, which affects protein structure and expression on the cell surface and results in subsequent intracellular accumulation. This leads to increased endoplasmic stress, upregulation of the unfolded protein response (UPR), and increased production of reactive oxygen species in mitochondria(5) resulting in enhanced activation of NF-κB and MAPK signalling and thus an increase in levels of proinflammatory cytokines (e.g. IL-1β, TNF, IL-6)(5-7). Persistent inflammation has been shown to have a strong impact on metabolic patterns. On the one hand, stimulated immune cells adapt their metabolism to provide sufficient energy for the proliferation and production of proinflammatory mediators. On the other hand, inflammatory responses are subject to regulation by metabolic pathway activity. Based on these aspects, gaining more insights into changes in metabolism in the context of TRAPS may facilitate the identification of both markers of disease activity and potential therapeutic targets. Consequently, we decided to use a mass spectrometry approach to study the changes in metabolic processes in three affected family members compared to age- and sex-matched healthy controls.

Methods

Genetic testing and *in silico* analyses of mutation – Next-generation sequencing was performed by SYNLAB Mannheim (https://www.synlab.de/lab/mannheim-genetik). For pathogenicity predictions of the mutation we, used the PolyPhen-2 web-software(8) and PROVEAN(9). Crystal structure 1 FT4 (10.1073/pnas.211178398)(10) obtained from the Protein Data Bank (www.rcsb.org) was modelled in PyMOL

(v2.5.4)(11). Subsequently, the Q111R mutation was generated to predict changes in the interactions between residues.

Metabolite extraction from plasma – Heparinized whole blood was obtained from study participants after written informed consent was given according to approval by the ethics committee (vote 12-240), University of Cologne, Cologne, Germany. The study is registered at the German Clinical Trials Registry under the ID: DRKS00010534. Plasma protein concentration was measured using a BCA kit (Thermo Fisher Scientific, Bremen, Germany). Metabolites were extracted using the Folch Method as described previously(12). Briefly, 200 µL of Chloroform and 150 µL of Methanol were added to the plasma. Samples were shaken for 1 h at 4 °C, followed by centrifugation at 3000 rcf for 10 min at 4 °C.

A volume of sample corresponding to 100 µg protein was collected and dried out using a speed vac. The samples were reconstituted in 10 µL of acetonitrile, and 5 µL was injected into the MS instrument.

Untargeted metabolomics – Analytes were separated using a UHPLC system (Vanquish, Thermo Fisher Scientific, Bremen, Germany) coupled to an HRAM mass spectrometer (Q-Exactive Plus, Thermo Fischer Scientific GmbH, Bremen, Germany) as described previously(13). Briefly, 2 µl of sample extract were injected into an X Select HSS T3 XP column, 100 Å, 2.5 µm, 2.1 mm x 100 mm (Waters), using a binary system comprised of 2 solutions, A: water with 0.1% formic acid, B: acetonitrile with 0.1% formic acid, operating at a flow rate of 0.1 mL/min and a column temperature kept at 30°C. Gradient elution was conducted as follows: isocratic step at 0.1% eluent B for 0.5 min, gradient increase up to 2% eluent B in 2 min, then increased up to 30% eluent B in 6 min and to 95% eluent B in 7 min, isocratic step at 95% eluent B for 2 min. The gradient was decreased to 0.1% eluent B in 3 min and held at 0.1% eluent B for 5 min. Mass spectra were recorded from 100-800 m/z at a mass resolution of 70,000 at m/z 400 in both positive and negative ion modes using data-dependent acquisition. Tandem mass spectra were acquired by performing CID. Sample injection order was randomised to minimise the effect of instrumental signal drift. MS data analysis was performed using Xcalibur software 4.0.

Compound identification and quantification – Metabolite search was performed using Compound discoverer 2.0 and mzCloud as online databases, considering

precursor ions with a deviation < 5 ppm, 0.5 min maximum retention time shift, minimum peak intensity 10^5, intensity tolerance 10, FT fragment mass tolerance 0.0025 Da, group covariance < 30%, p-value < 0.05 and area Max ≥ 10000. Metabolites were considered to be correctly identified when at least two specific fragments were found in the MS2 spectra. Quantification was performed using Trace finder 4.1, genesis detection algorithm, nearest RT, S/N threshold 8, min peak height (S/N) equal to 3, peak S/N cut-off 2.00, valley rise 2%, valley S/N 1.10. Relative quantification was obtained by dividing the area of individual metabolites to spiked internal standards (Leucine enkephalin, myristic acid and cysteamine sodium salt).

Statistical analyses – Quantified metabolites were analysed using the inbuilt tools of the MetaboAnalyst platform (metaboanalyst.ca)(14). Changes in single metabolites were classified as significant when log2FC > 0.5 and t-Test returned both p < 0.05 and false discovery rate (FDR) < 0.05 (Suppl. Tab. S1, available at *Rheumatology* online). The quantitative enrichment analysis and pathway analysis modules were used for pathway analyses (Suppl. Tab. S2 and S3, available at *Rheumatology* online).

Measurements of inflammatory markers – C-reactive protein (CRP) was determined by the CRP Latex Test Gen. 3, a particle-enhanced immunoturbidimetry (Roche Diagnostics®) with the Cobas C702 analyser system. Interleukin 6 (IL-6) was determined by the Elecsys IL-6 (Roche Diagnostics®), a sandwich immunoassay, using the Cobas E801 analyser system.

Case description and Results

A 44-year-old man (patient 1) presented to our hospital with abdominal pain, highly elevated inflammation parameters and chronic kidney disease with severe proteinuria KDIGO G5A3 (Figure 1A). Kidney biopsy showed severe AA-amyloidosis (Figure 2). Patient history revealed recurrent attacks of abdominal pain with fever and elevation of inflammatory markers such as C-reactive protein (CRP) that had first occurred at the age of 16 years. He also reported that his father, aunt, sister and daughter had similar problems (Figure 1B).

His 19-year-old daughter (patient 2) disclosed that she had had recurrent episodes of abdominal pain with a fever of up to 38.5 °C since she was 11 years old (Figure 1A, B). The attacks lasted > 14 days and occurred 3-5 times a year. Due to the recurrent

abdominal pain attacks, she had already had an appendectomy at the age of 15 years and had undergone a diagnostic laparoscopy, where endometriosis was suspected, but only signs of unspecific peritonitis were evident. She denied skin rashes during the attacks. At the time of her presentation to our department, she showed highly elevated CRP levels (263 mg/dl) but only reported mild abdominal pain when asked. Kidney function was normal, and proteinuria was within normal range. The 46-year-old sister of patient 1 (patient 3) also presented with a history of recurrent abdominal pain and fever at 6-8 weeks intervals since the age of 12 years (Figure 1A, B). She also reported suffering from cervical lymphadenopathy and arthralgia during the attacks. On presentation, she showed mildly impaired kidney function (eGFR 63 ml/min) and proteinuria of 2000 mg/g creatinine (albuminuria 1500 mg/g creatinine), strongly suggesting early renal AA amyloidosis.

All five symptomatic family members underwent genetic testing that revealed the TNFRSF1A-variant c.332A>G (p.Q111R) (Figure 1C). To our knowledge, this missense variant has not yet been reported in the literature or the infevers database(15, 16). *In silico* analyses of the mutation by PolyPhen-2 software(8) and Provean(9) classified the mutation as probably damaging (score: 0.999) and deleterious (Provean-Score: -3.541), respectively. *In silico* analysis via the PyMOL software(11) and the Project HOPE server(17) was performed to obtain three-dimensional representations of the protein (Figure 3A). Modelling of the mutation revealed that the mutant residue (Q111R) is larger than the wild-type residue and is positively charged, whereas the wild-type is neutral. Unlike wild-type (Figure 3B), mutant residues cannot form hydrogen bonds with the backbone carbonyl group R106 likely affecting the proper folding of this domain (Figure 3C). The mutation is located in the cysteine-rich domain 2 (CRD 2) of the protein's extracellular domain, where most TRAPS-causing mutations are reported (Figure 1C)(5).

Taking into account the typical clinical picture, the histological evidence of renal AA amyloidosis, the detection of a mutation in the TNFRSF1A gene and the fact that the mutation was found in the extracellular domain of TNR1A, the diagnosis of TRAPS was made.

All patients received the IL-1β inhibitor canakinumab for treatment, and all responded with normalisation of inflammatory parameters and clinical remission. Figure 1A shows

the clinical characteristics and laboratory results of all patients. Notably, patient 3 showed a marked decrease in proteinuria during treatment with canakinumab, which we interpret as an improvement in suspected early renal AA amyloidosis. While the proinflammatory changes and the pathophysiological changes in TNFα signalling have been well described, the impact of these mutations on metabolism has not been sufficiently studied to date(7, 18) Thus, we used mass spectrometry to test metabolomic changes in the patients.

Figure 4A shows a heatmap of metabolic changes in the plasma of our three patients during disease flares and during remission (defined by the absence of clinical symptoms and normal levels of CRP as well as IL-6 (Figure 5C)) compared to age- and sex-matched healthy controls. We found 31 metabolites upregulated and 35 compounds downregulated (Suppl. Tab.S1).

Intriguingly, these metabolic changes seemed to be independent of disease activity (Figure 4A, Figure 5A).

Among the significantly upregulated metabolites, we identified hypoxanthine, kynurenine, phenylalanine and choline (Figure 4B), while tryptophan, arginine, tyrosine and methionine were found to be among the significantly downregulated metabolites (Figure 4C).

Quantitative enrichment analyses revealed that arginine biosynthesis and tryptophan metabolism were among the most enriched pathways according to the KEGG library (Figure 4D, Suppl. Tab. S2).

Sparse partial least-squares discriminant analysis (sPLS-DA) confirmed a distinct signature for all patients compared to healthy controls, while no differences were evident concerning disease activity (Figure 4E). Notably, arginine biosynthesis and biosynthesis of phenylalanine, tyrosine and tryptophan also scored high when quantifying the impact of KEGG pathways using pathway enrichment analyses. In addition, cysteine and methionine metabolism emerged as another impactful pathway (Figure 5B, Suppl. Tab. S3).

Discussion:

We present a novel TNFRSF1A-variant c.332A>G (p.Q111R) causing TRAPS in affected patients. We observed a remarkable response with normalisation of inflammatory parameters in all three patients upon initiating treatment with the IL-1β antibody canakinumab. Furthermore, we interpret the near normalisation of proteinuria in patient 3 as regressive amyloidosis of the kidney. This is in line with findings that early intervention targeting the IL-1 pathway can stop or improve the course of renal amyloidosis in patients with familial Mediterranean fever(19).

In contrast to the effects of canakinumab on inflammation, the metabolomic signature did not correlate with disease activity. This can be considered analogous to observations from TRAPS patients, where blocking the action of proinflammatory cytokines associated with TRAPS (e.g., IL-1, TNF) could improve clinical symptoms but did not affect the underlying activation of intracellular inflammatory signalling pathways(20).

Many affected pathways, such as arginine biosynthesis (Figure 5D) and tryptophan metabolism, have been described as dysregulated in inflammation (reviewed in Ref.(21)). In humans, Indoleamine 2,3 dioxygenase (IDO) catabolises the initial steps of a series of reactions leading to the conversion of tryptophan to kynurenine. These reactions seem activated in inflammation, with the tryptophan/kynurenine ratio being suggested as a marker for infectious diseases such as COVID-19(22, 23). Interestingly, it has been shown that proinflammatory cytokines may prime macrophages and dendritic cells to express IDO and release reactive oxygen species (ROS), leading to the conversion of tryptophan to kynurenine and inhibiting the conversion of phenylalanine to tyrosine, respectively (Figure 5E)(24, 25).

In addition, activated macrophages have also been studied regarding choline metabolism, which was enriched in all patients (Figure 4B). For example, it has been shown that activated murine macrophages can enhance choline uptake, increasing IL-1 and IL-18 production(26). Furthermore, dietary supplementation of choline in mice led to upregulation of the scavenger factor CD36(27). Murine macrophages deficient in CD36 have been shown to display downregulation of proinflammatory cytokines and reduced oxidative stress (28, 29). The notion that increased choline levels contribute to the disease phenotype is supported by findings in a mouse model of Muckle-Wells syndrome, a different periodic fever syndrome. Here the absence of choline led to a reduction in disease severity(26). In humans, both beneficial and harmful effects of

choline have been described. A study analysing the metabolic profile changes in the plasma of patients diagnosed with inflammatory rheumatoid arthritis found choline to be increased(30). Conversely, choline has been described to attenuate immune activity in asthma patients and to ameliorate cardiovascular damage by inhibiting the inflammatory response in rats(31, 32).

It is noteworthy that choline is linked to methionine metabolism, which we observed to be among the most impactful pathways to be dysregulated (Figure 5B, F). Betaine, a choline derivative, is required to convert homocysteine to methionine(33). Indeed, we noted upregulation of homocysteine while methionine appeared downregulated (Figure 4C, Suppl. Tab. S1). In line with this, we also detected the downregulation of S-adenosyl-methionine which is produced in the conversion of methionine to homocysteine (Figure 5F)(34). Homocysteine synthesis from methionine also leads to adenosine production, which is subsequently converted to hypoxanthine (Figure 5F)(35). Hypoxanthine can then be oxidised to xanthine and uric acid in ensuing reactions (Figure 5F). Of note we found hypoxanthine to be highly enriched while both adenosine and xanthine were slightly decreased; however, not to a level of log2FC > 0.5. In the context of cancer, increased production of purines from hypoxanthine has been described to suppress immune function through downregulation of IL-1β in the tumour microenvironment(36). We interpret the enrichment of hypoxanthine in our data to be a reflection of TRAPS-induced hyperactivation of immune cells.

Hyperhomocysteinemia has been well-described for cardiovascular diseases and rheumatoid arthritis(37, 38). In addition, homocysteine has also been shown to drive inflammation through macrophage activation(33). In microglia, resident brain macrophages, homocysteine leads to activation and subsequent release of inflammatory factors such as TNF-α and IL-6(39).

All of these changes in metabolite abundance can be observed in the context of oxidative stress. We found oxidised glutathione (GSSG) to be significantly increased and reduced glutathione (GSH) to be significantly decreased, yielding an increased ratio indicative of oxidative stress (Suppl. Tab. 1, Figure 5F)(40). Furthermore, increased ROS production – the cause of oxidative stress – has been shown in TRAPS patients independent of disease activity(6). Thus, we speculate that the overactivation

of macrophages in the context of oxidative stress might be one of the mechanisms underlying the observed metabolic changes.

However, further mechanistic studies are needed to elucidate why changes in the metabolome consistent with inflammation do not appear to correlate with clinical symptoms or laboratory parameters of disease activity. This is particularly striking since after treatment of 20 TRAPS patients with canakinumab, many genes relevant to disease pathogenesis moved towards levels seen in the healthy volunteers(41). Our findings imply that the metabolic changes are not conclusively explained by the phenotypic proinflammatory cytokines but rather seem to be an effect of mutation-associated changes in other pathways that are not affected by treatment with canakinumab. It is conceivable that this also applies to other monogenetic autoinflammatory diseases that have a similar inflammatory phenotype and responsiveness to IL-1 inhibitors.

Despite the successful clinical response and the significant changes observed in the metabolome, this study was limited because only three family members were available for testing, which is typical in rare genetic disorders. Further studies are needed to confirm our findings and to clarify whether these results are mutation-specific or can be generalised to other known TRAPS-causing mutations or even to other known monogenic autoinflammatory fever syndromes.

Conclusion:

Here we present a novel mutation in the TNFRSF1A gene that causes TRAPS and is associated with AA-amyloidosis. Canakinumab is an effective treatment in this variant and led to improvement in proteinuria in one of the patients with presumed early renal AA-amyloidosis. We observed significant changes in the metabolome compared to healthy controls affecting several pathways, most prominently arginine biosynthesis, tryptophan metabolism and metabolism of cysteine and methionine. Treatment with canakinumab did not appear to affect these metabolic changes caused by TRAPS. Further studies are needed to examine how these pathways, which seem unaffected by treatment with canakinumab, contribute to the pathophysiology of TRAPS.

Funding

This work was supported by funding from the European Research Council (ERC) under the European Union's Horizon 2020 research and innovation programme (grant agreement No 834259).

J.D.S., An.A., R.L., and A.A. were supported by the Max-Planck-Gesellschaft (MPG).

Conflict of interest

The authors have declared no conflict of interest.

Data availability

The datasets generated during and/or analysed during the current study are available from the corresponding author on reasonable request.

Ethics

The study was conducted in accordance with the Declaration of Helsinki, and samples were collected and analysed under protocols approved by the ethics committee (vote 12-240), University of Cologne, Cologne, Germany. The study is registered at the German Clinical Trials Registry under the ID: DRKS00010534. Informed consent was received.

Acknowledgements

We thank Nadine Hochhard and Christian Latza for technical support.

References

1. McDermott MF, Aksentijevich I, Galon J, McDermott EM, Ogunkolade BW, Centola M, et al. Germline Mutations in the Extracellular Domains of the 55 kDa TNF Receptor, TNFR1, Define a Family of Dominantly Inherited Autoinflammatory Syndromes. Cell. 1999;97(1):133-44.
2. Hull KM, Drewe E, Aksentijevich I, Singh HK, Wong K, McDermott EM, et al. The TNF receptor-associated periodic syndrome (TRAPS): emerging concepts of an autoinflammatory disorder. Medicine (Baltimore). 2002;81(5):349-68.
3. Lachmann HJ, Papa R, Gerhold K, Obici L, Touitou I, Cantarini L, et al. The phenotype of TNF receptor-associated autoinflammatory syndrome (TRAPS) at presentation: a series of 158 cases from the Eurofever/EUROTRAPS international registry. Ann Rheum Dis. 2014;73(12):2160-7.
4. Lainka E, Neudorf U, Lohse P, Timmann C, Stojanov S, Huss K, et al. Incidence of TNFRSF1A mutations in German children: epidemiological, clinical and genetic characteristics. Rheumatology (Oxford). 2009;48(8):987-91.

5. Cudrici C, Deuitch N, Aksentijevich I. Revisiting TNF Receptor-Associated Periodic Syndrome (TRAPS): Current Perspectives. Int J Mol Sci. 2020;21(9).
6. Bulua AC, Simon A, Maddipati R, Pelletier M, Park H, Kim KY, et al. Mitochondrial reactive oxygen species promote production of proinflammatory cytokines and are elevated in TNFR1-associated periodic syndrome (TRAPS). J Exp Med. 2011;208(3):519-33.
7. Simon A, Park H, Maddipati R, Lobito AA, Bulua AC, Jackson AJ, et al. Concerted action of wild-type and mutant TNF receptors enhances inflammation in TNF receptor 1-associated periodic fever syndrome. Proceedings of the National Academy of Sciences of the United States of America. 2010;107(21):9801-6.
8. Adzhubei IA, Schmidt S, Peshkin L, Ramensky VE, Gerasimova A, Bork P, et al. A method and server for predicting damaging missense mutations. Nat Methods. 2010;7(4):248-9.
9. Choi Y, Chan AP. PROVEAN web server: a tool to predict the functional effect of amino acid substitutions and indels. Bioinformatics. 2015;31(16):2745-7.
10. Carter PH, Scherle PA, Muckelbauer JK, Voss ME, Liu RQ, Thompson LA, et al. Photochemically enhanced binding of small molecules to the tumor necrosis factor receptor-1 inhibits the binding of TNF-alpha. Proceedings of the National Academy of Sciences of the United States of America. 2001;98(21):11879-84.
11. Schrödinger LaWD. The PyMOL Molecular Graphics System, Version 2.5.4. 2020.
12. Patterson RE, Ducrocq AJ, McDougall DJ, Garrett TJ, Yost RA. Comparison of blood plasma sample preparation methods for combined LC-MS lipidomics and metabolomics. J Chromatogr B Analyt Technol Biomed Life Sci. 2015;1002:260-6.
13. Annibal A, Tharyan RG, Schonewolff MF, Tam H, Latza C, Auler MMK, et al. Regulation of the one carbon folate cycle as a shared metabolic signature of longevity. Nat Commun. 2021;12(1):3486.
14. Pang Z, Zhou G, Ewald J, Chang L, Hacariz O, Basu N, et al. Using MetaboAnalyst 5.0 for LC–HRMS spectra processing, multi-omics integration and covariate adjustment of global metabolomics data. Nature Protocols. 2022;17(8):1735-61.
15. Milhavet F, Cuisset L, Hoffman HM, Slim R, El-Shanti H, Aksentijevich I, et al. The infevers autoinflammatory mutation online registry: update with new genes and functions. Hum Mutat. 2008;29(6):803-8.
16. Van Gijn ME, Ceccherini I, Shinar Y, Carbo EC, Slofstra M, Arostegui JI, et al. New workflow for classification of genetic variants' pathogenicity applied to hereditary recurrent fevers by the International Study Group for Systemic Autoinflammatory Diseases (INSAID). J Med Genet. 2018;55(8):530-7.
17. Venselaar H, Te Beek TA, Kuipers RK, Hekkelman ML, Vriend G. Protein structure analysis of mutations causing inheritable diseases. An e-Science approach with life scientist friendly interfaces. BMC Bioinformatics. 2010;11:548.
18. Nowlan ML, Drewe E, Bulsara H, Esposito N, Robins RA, Tighe PJ, et al. Systemic cytokine levels and the effects of etanercept in TNF receptor-associated periodic syndrome (TRAPS) involving a C33Y mutation in TNFRSF1A. Rheumatology (Oxford). 2006;45(1):31-7.
19. Ugurlu S, Ergezen B, Egeli BH, Selvi O, Ozdogan H. Safety and efficacy of anti-interleukin-1 treatment in 40 patients, followed in a single centre, with AA amyloidosis secondary to familial Mediterranean fever. Rheumatology (Oxford). 2020;59(12):3892-9.
20. Negm OH, Mannsperger HA, McDermott EM, Drewe E, Powell RJ, Todd I, et al. A pro-inflammatory signalome is constitutively activated by C33Y mutant TNF receptor 1 in TNF receptor-associated periodic syndrome (TRAPS). Eur J Immunol. 2014;44(7):2096-110.
21. Lemos H, Huang L, Prendergast GC, Mellor AL. Immune control by amino acid catabolism during tumorigenesis and therapy. Nature Reviews Cancer. 2019;19(3):162-75.
22. Lionetto L, Ulivieri M, Capi M, De Bernardini D, Fazio F, Petrucca A, et al. Increased kynurenine-to-tryptophan ratio in the serum of patients infected with SARS-CoV2: An observational cohort study. Biochimica et Biophysica Acta (BBA) - Molecular Basis of Disease. 2021;1867(3):166042.
23. Sorgdrager FJH, Naudé PJW, Kema IP, Nollen EA, Deyn PP. Tryptophan Metabolism in Inflammaging: From Biomarker to Therapeutic Target. Front Immunol. 2019;10:2565.

24. Capuron L, Schroecksnadel S, Féart C, Aubert A, Higueret D, Barberger-Gateau P, et al. Chronic low-grade inflammation in elderly persons is associated with altered tryptophan and tyrosine metabolism: role in neuropsychiatric symptoms. Biol Psychiatry. 2011;70(2):175-82.
25. Yanagawa Y, Iwabuchi K, Onoé K. Co-operative action of interleukin-10 and interferon-gamma to regulate dendritic cell functions. Immunology. 2009;127(3):345-53.
26. Sanchez-Lopez E, Zhong Z, Stubelius A, Sweeney SR, Booshehri LM, Antonucci L, et al. Choline Uptake and Metabolism Modulate Macrophage IL-1β and IL-18 Production. Cell metabolism. 2019;29(6):1350-62.e7.
27. Wang Z, Klipfell E, Bennett BJ, Koeth R, Levison BS, Dugar B, et al. Gut flora metabolism of phosphatidylcholine promotes cardiovascular disease. Nature. 2011;472(7341):57-63.
28. Okamura DM, Pennathur S, Pasichnyk K, López-Guisa JM, Collins S, Febbraio M, et al. CD36 regulates oxidative stress and inflammation in hypercholesterolemic CKD. J Am Soc Nephrol. 2009;20(3):495-505.
29. Cai L, Wang Z, Ji A, Meyer JM, van der Westhuyzen DR. Scavenger receptor CD36 expression contributes to adipose tissue inflammation and cell death in diet-induced obesity. PloS one. 2012;7(5):e36785-e.
30. Coras R, Murillo-Saich JD, Guma M. Circulating Pro- and Anti-Inflammatory Metabolites and Its Potential Role in Rheumatoid Arthritis Pathogenesis. Cells. 2020;9(4):827.
31. Mehta AK, Singh BP, Arora N, Gaur SN. Choline attenuates immune inflammation and suppresses oxidative stress in patients with asthma. Immunobiology. 2010;215(7):527-34.
32. Liu L, Lu Y, Bi X, Xu M, Yu X, Xue R, et al. Choline ameliorates cardiovascular damage by improving vagal activity and inhibiting the inflammatory response in spontaneously hypertensive rats. Scientific Reports. 2017;7(1):42553.
33. Chiuve SE, Giovannucci EL, Hankinson SE, Zeisel SH, Dougherty LW, Willett WC, et al. The association between betaine and choline intakes and the plasma concentrations of homocysteine in women. Am J Clin Nutr. 2007;86(4):1073-81.
34. Durand P, Prost M, Loreau N, Lussier-Cacan S, Blache D. Impaired Homocysteine Metabolism and Atherothrombotic Disease. Laboratory Investigation. 2001;81(5):645-72.
35. Bajic Z, Sobot T, Skrbic R, Stojiljkovic MP, Ponorac N, Matavulj A, et al. Homocysteine, Vitamins B6 and Folic Acid in Experimental Models of Myocardial Infarction and Heart Failure—How Strong Is That Link? Biomolecules [Internet]. 2022; 12(4).
36. Townsend MH, Tellez Freitas CM, Larsen D, Piccolo SR, Weber KS, Robison RA, et al. Hypoxanthine Guanine Phosphoribosyltransferase expression is negatively correlated with immune activity through its regulation of purine synthesis. Immunobiology. 2020;225(3):151931.
37. Guieu R, Ruf J, Mottola G. Hyperhomocysteinemia and cardiovascular diseases. Ann Biol Clin (Paris). 2022;80(1):7-14.
38. Roubenoff R, Dellaripa P, Nadeau MR, Abad LW, Muldoon BA, Selhub J, et al. Abnormal homocysteine metabolism in rheumatoid arthritis. Arthritis & Rheumatism. 1997;40(4):718-22.
39. Chen S, Dong Z, Cheng M, Zhao Y, Wang M, Sai N, et al. Homocysteine exaggerates microglia activation and neuroinflammation through microglia localized STAT3 overactivation following ischemic stroke. J Neuroinflammation. 2017;14(1):187.
40. Diaz-Vivancos P, de Simone A, Kiddle G, Foyer CH. Glutathione--linking cell proliferation to oxidative stress. Free Radic Biol Med. 2015;89:1154-64.
41. Torene R, Nirmala N, Obici L, Cattalini M, Tormey V, Caorsi R, et al. Canakinumab reverses overexpression of inflammatory response genes in tumour necrosis factor receptor-associated periodic syndrome. Annals of the rheumatic diseases. 2017;76(1):303-9.

Figure 1 Three patients presenting with a novel TRAPS causing mutation

A Patient characteristics and selected laboratory markers at initial presentation and at follow up visit. CRP (C-reactive protein), SAA (Serum Amyloid A), eGFR (estimated glomerular filtration rate (estimated using FAS equation)). **B** Pedigree of patient family. Patients denoted as 1, 2 and 3, respectively, presented to our hospital. **C** Schematic representation of the mutation in exon 4 of the TNFRSF1A gene present in all three patients and of the ensuing amino acid substitution at protein level. Cys (cysteine rich region), NSD (N-SMASE activation domain), Death (Death Domain).

Figure 2 Histology of kidney of patient 1 reveals renal AA-amyloidosis

A Light microscopy of the kidney shows deposits of amorphous material in glomeruli and arterioles (marked by black arrows). Periodic acid–Schiff (PAS) stain. **B** Congo red staining identify deposits as amyloid (marked by black arrows). **C** Polarized light microscopy identify deposits as amyloid (marked by white arrows). **D** Electron microscopy overview (magnification 2100x) of a glomerulus shows cloudy structures. **E** Higher magnification (46400x) of D shows cloudy structure are identifiable as amyloid fibrils.

Figure 3 Crystal structure of TNR1A reveals disruption of hydrogen bonds

A Cartoon representation of dimeric TNR1A (PDB 1FT4); one monomer is coloured in deep teal, and the second monomer is in deep purple. **B** Magnification of the region containing Q111 and neighbouring interacting residues R106 and F141 shown in sticks. Carbons are colour coded in grey, nitrogen in blue and oxygen in red. Hydrogen bonds are depicted as yellow dashed lines. **C** Q111R mutation disrupts the interaction with the backbone carbonyl group R106, likely affecting the proper folding of this domain. Images were generated with PyMOL (v2.5.4)(1).

Figure 4 Plasma metabolome of TRAPS patients is dysregulated compared to healthy controls

A Untargeted metabolomic analysis of three patients compared with eight age- and sex-matched healthy controls. For patients 1 and 2, samples obtained during active disease flares (A) and during remission (R) were analysed. Heat map depicting log2 transformed abundance of metabolites (normalized to internal standard) relative to average of controls (listed in Suppl. Table 1). Metabolites and samples were hierarchically clustered using Euclidean metrics. **B** Relative abundance of hypoxanthine, L-kynurenine, L-phenylalanine and choline in TRAPS patients compared to healthy controls. Blue symbols denote patient 1, purple symbols patient 2 and green patient 3. Circles denote disease in remission while triangles denote active disease. Significance was assessed using unpaired t-test: **** $p<0.0001$ and * $p<0.05$. **C** Relative abundance of L-tryptophan, L-arginine, L-tyrosine and L-methionine in TRAPS patients compared to healthy controls. Blue symbols denote patient 1, purple symbols patient 2 and green patient 3. Circles denote disease in remission while triangles denote active disease. Significance was assessed using unpaired t-test: **** $p<0.0001$. **D** Quantitative enrichment analysis obtained by uploading all quantified metabolites to MetaboAnalyst (https://www.metaboanalyst.ca)(2) in the three patients compared to healthy control. Only pathways featuring at least five entries were considered. KEGG pathways containing 84 metabolite sets (KEGG, Oct. 2019) was selected. Detailed parameters are shown in Supplementary Table S2. **E** Sparse partial least squared- discriminant analysis (sPLS-DA) scores of the untargeted metabolomic features of all five conditions compared to healthy controls obtained by MetaboAnalyst

(https://www.metaboanalyst.ca)(2). Component 1, X axis, Component 2, Y axis. Both components are comprised of ten features each. In the score plot ellipses correspond to 95% confidence region.

Figure 5 Metabolome of TRAPS patients is independent of disease activity

A Untargeted metabolomic analysis of patients 1 and 2 during active disease flares (A) and during remission (R). Heat map depicting log2 transformed abundance of metabolites (normalized to internal standard) relative to average of controls (listed in Suppl. Table S1). Metabolites and samples were hierarchically clustered using Euclidean metrics. **B** Pathway analysis obtained by uploading all quantified metabolites to MetaboAnalyst (https://www.metaboanalyst.ca)(2) in the three patients compared to healthy control. Only pathways featuring at least five entries were considered. KEGG pathways containing 84 metabolite sets (KEGG, Oct. 2019) was selected. Pathways with highest impact scores were annotated. Detailed parameters are shown in Supplementary Table S3. **C** Inflammatory markers measured during active disease and during remission. Serum levels of C-reactive protein (CRP) were measured using particle-enhanced immunoturbidimetry and levels of interleukin 6 (IL-6) were determined by the Elecsys IL-6 (Roche Diagnostics®), a sandwich immunoassay, using the Cobas E801 analyser system. **D** Schematic representation of the arginine biosynthesis pathway as considered for the pathway analysis in B. Red rectangles denote metabolites significantly downregulated, grey rectangles denote metabolites not significantly changed and green rectangles denote metabolites significantly upregulated when comparing patients to healthy controls. **E** Schematic representation of basic mechanisms by which monocytes/macrophages/dendritic cells can influence selected pathways. ROS=reactive oxygen species, IDO=Indoleamine 2,3-dioxygenase 1 Modified from Ref. (3). **F** Schematic representation of the homocysteine/methionine pathway and its interplay with choline and hypoxanthine metabolism as well as biosynthesis of GSH. Red and green rectangles denote metabolites significantly upregulated and downregulated, respectively. Hatched red rectangles and hatched green denote metabolites significantly upregulated and downregulated, respectively, but failing to reach log2FC > 0.5. Grey rectangles denote metabolites not significantly changed when comparing patients to healthy controls. Hatched grey rectangles denote metabolites not measured in our dataset. SA methionine=S-adenosylmethionine, SA-homocysteine=S-adenosylhomocysteine, THF=tetrahydrofolic acid, 5-Met-THF=5-methyltetrahydrofolic acid, CDP-Choline=cytidine-5'-diphosphocholine, GSH= glutathione, GSSG= oxidised glutathione. Adapted from Refs. (4-6)

A

		Patient 1	Patient 2	Patient 3
Patient characteristics	*Gender*	M	F	F
	Age (y)	45	19	47
	Age at onset (y)	16	11	12
	Symptoms	abdominal pain; fever; arthralgia	abdominal pain; fever	abdominal pain; fever; lymphadenopathy; arthralgia
	Attack duration (d)	> 14	> 14	> 14
	Histology	Renal AA amyloidosis	N/A	N/A
Medical treatment	*First 6 months*	Canakinumab 150 mg every 4 weeks	Canakinumab 150 mg once at first visit	Canakinumab 150 mg every 4 weeks
Selected laboratory parameters at initial presentation	*CRP (mg/l)*	89	263	65
	SAA (mg/dl)	78.9	155	74
	Creatinine (mg/dl)	4.9	0.74	1.1
	eGFR (ml/min)	13	100	63
	Albuminuria (mg/g creatinine)	4367	4	1574
Selected laboratory parameters at follow-up presentation	*CRP (mg/l)*	2.1	4.7	0.9
	SAA (mg/dl)	0.86	0.39	0.56
	Creatinine (mg/dl)	6.5	0.83	1.2
	eGFR (ml/min)	14	90	58
	Albuminuria (mg/g creatinine)	3000	4	175

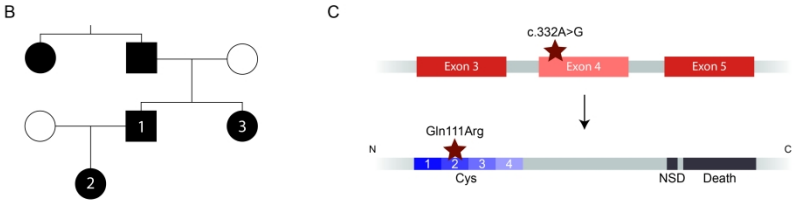

Figure 1 Three patients presenting with a novel TRAPS causing mutation
A Patient characteristics and selected laboratory markers at initial presentation and at follow up visit. CRP (C-reactive protein), SAA (Serum Amyloid A), eGFR (estimated glomerular filtration rate (estimated using FAS equation)).
B Pedigree of patient family. Patients denoted as 1, 2 and 3, respectively, presented to our hospital.
C Schematic representation of the mutation in exon 4 of the TNFRSF1A gene present in all three patients and of the ensuing amino acid substitution at protein level. Cys (cysteine rich region), NSD (N-SMASE activation domain), Death (Death Domain).

210x297mm (600 x 600 DPI)

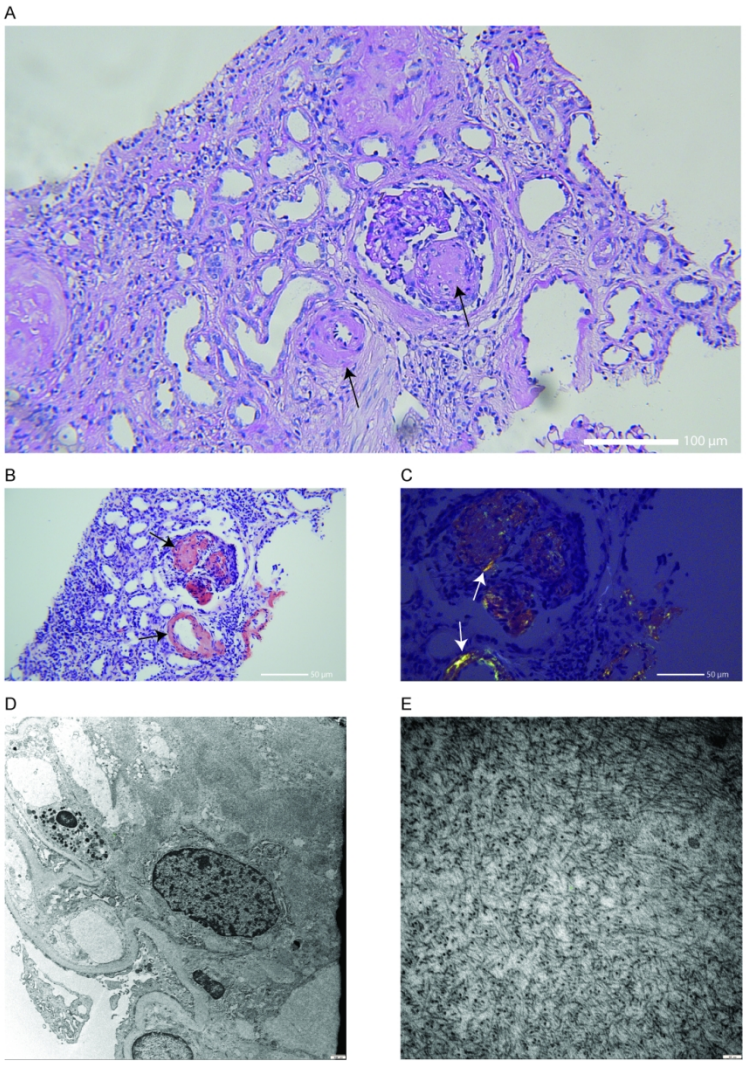

Figure 2 Histology of kidney of patient 1 reveals renal AA-amyloidosis
A Light microscopy of the kidney shows deposits of amorphous material in glomeruli and arterioles (marked by black arrows). Periodic acid–Schiff (PAS) stain.
B Congo red staining identify deposits as amyloid (marked by black arrows).
C Polarized light microscopy identify deposits as amyloid (marked by white arrows).
D Electron microscopy overview (magnification 2100x) of a glomerulus shows cloudy structures.
E Higher magnification (46400x) of D shows cloudy structure are identifiable as amyloid fibrils.

210x297mm (150 x 150 DPI)

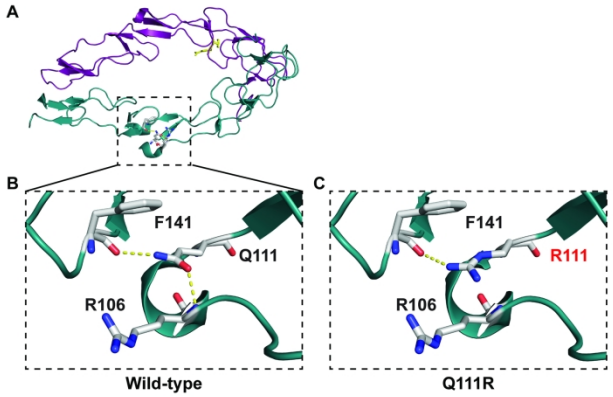

Figure 3 Crystal structure of TNR1A reveals disruption of hydrogen bonds
A Cartoon representation of dimeric TNR1A (PDB 1FT4); one monomer is coloured in deep teal, and the second monomer is in deep purple.
B Magnification of the region containing Q111 and neighbouring interacting residues R106 and F141 shown in sticks. Carbons are colour coded in grey, nitrogen in blue and oxygen in red. Hydrogen bonds are depicted as yellow dashed lines.
C Q111R mutation disrupts the interaction with the backbone carbonyl group R106, likely affecting the proper folding of this domain. Images were generated with PyMOL (v2.5.4)(1).

209x296mm (300 x 300 DPI)

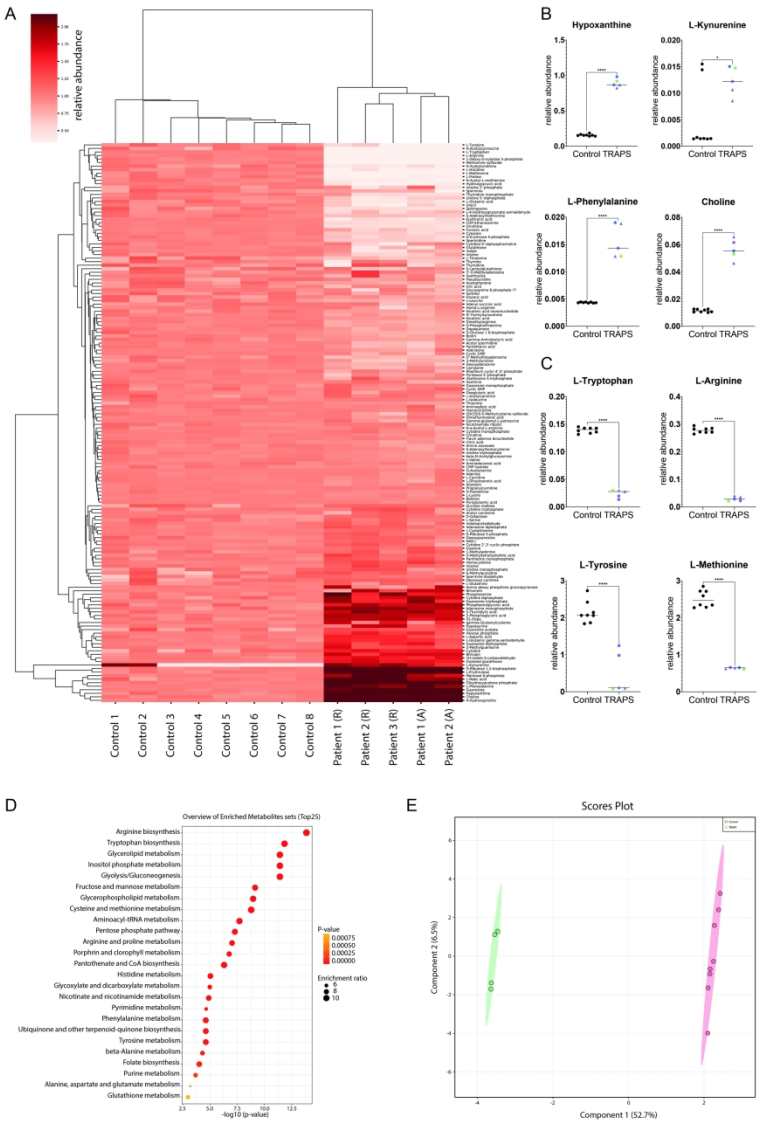

Figure 4 Plasma metabolome of TRAPS patients is dysregulated compared to healthy controls

A Untargeted metabolomic analysis of three patients compared with eight age- and sex-matched healthy controls. For patients 1 and 2, samples obtained during active disease flares (A) and during remission (R) were analysed. Heat map depicting log2 transformed abundance of metabolites (normalized to internal standard) relative to average of controls (listed in Suppl. Table 1). Metabolites and samples were hierarchically clustered using Euclidean metrics.

B Relative abundance of hypoxanthine, L-kynurenine, L-phenylalanine and choline in TRAPS patients compared to healthy controls. Blue symbols denote patient 1, purple symbols patient 2 and green patient 3. Circles denote disease in remission while triangles denote active disease. Significance was assessed using unpaired t-test: **** $p<0.0001$ and * $p<0.05$.

C Relative abundance of L-tryptophan, L-arginine, L-tyrosine and L-methionine in TRAPS patients compared to healthy controls. Blue symbols denote patient 1, purple symbols patient 2 and green patient 3. Circles denote disease in remission while triangles denote active disease. Significance was assessed using unpaired t-test: **** $p<0.0001$.

D Quantitative enrichment analysis obtained by uploading all quantified metabolites to MetaboAnalyst (https://www.metaboanalyst.ca)(2) in the three patients compared to healthy control. Only pathways featuring at least five entries were considered. KEGG pathways containing 84 metabolite sets (KEGG, Oct. 2019) was selected. Detailed parameters are shown in Supplementary Table 2.
E Sparse partial least squared- discriminant analysis (sPLS-DA) scores of the untargeted metabolomic features of all five conditions compared to healthy controls obtained by MetaboAnalyst (https://www.metaboanalyst.ca)(2). Component 1, X axis, Component 2, Y axis. Both components are comprised of ten features each. In the score plot ellipses correspond to 95% confidence region.

210x297mm (300 x 300 DPI)

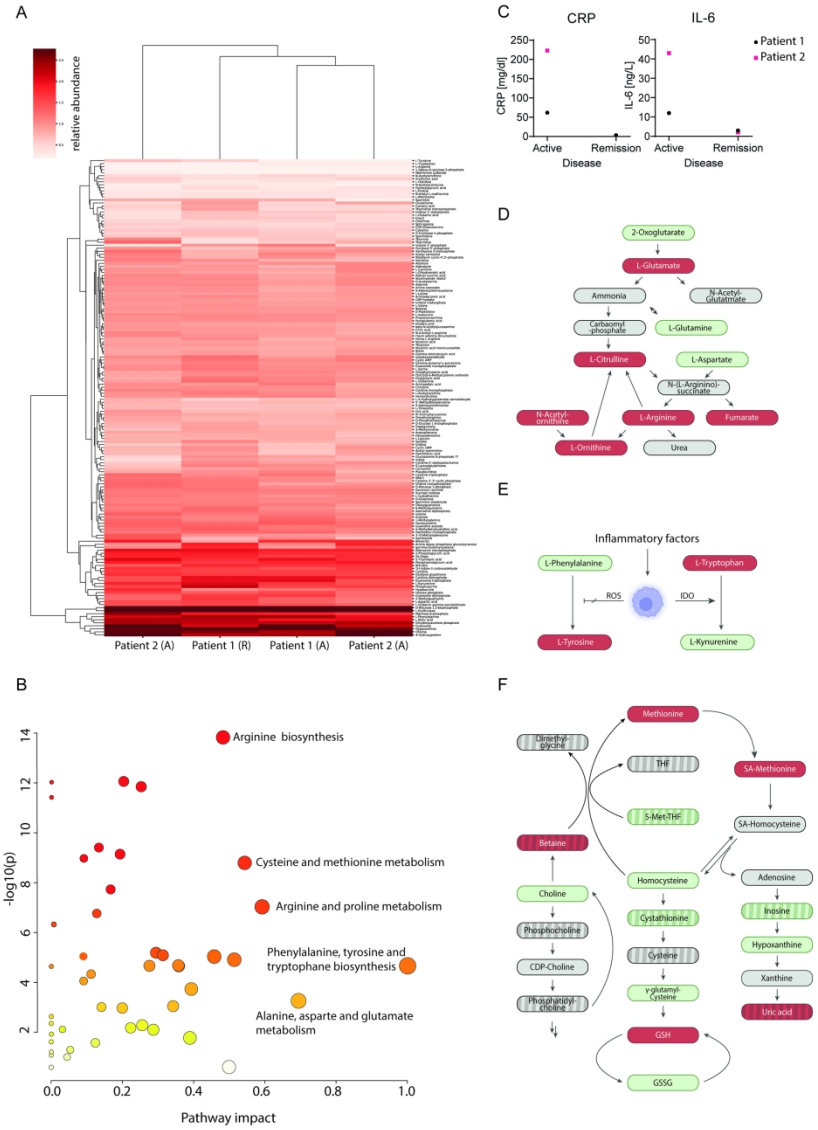

Figure 5 Metabolome of TRAPS patients is independent of disease activity

A Untargeted metabolomic analysis of patients 1 and 2 during active disease flares (A) and during remission (R). Heat map depicting log2 transformed abundance of metabolites (normalized to internal standard) relative to average of controls (listed in Suppl. Table 1). Metabolites and samples were hierarchically clustered using Euclidean metrics.

B Pathway analysis obtained by uploading all quantified metabolites to MetaboAnalyst (https://www.metaboanalyst.ca)(2) in the three patients compared to healthy control. Only pathways featuring at least five entries were considered. KEGG pathways containing 84 metabolite sets (KEGG, Oct. 2019) was selected. Pathways with highest impact scores were annotated. Detailed parameters are shown in Supplementary Table 3.

C Inflammatory markers measured during active disease and during remission. Serum levels of C-reactive protein (CRP) were measured using particle-enhanced immunoturbidimetry and levels of interleukin 6 (IL-6) were determined by the Elecsys IL-6 (Roche Diagnostics®), a sandwich immunoassay, using the Cobas E801 analyser system.

D Schematic representation of the arginine biosynthesis pathway as considered for the pathway analysis in B. Red rectangles denote metabolites significantly downregulated, grey rectangles denote metabolites not significantly changed and green rectangles denote metabolites significantly upregulated when comparing patients to healthy controls.
E Schematic representation of basic mechanisms by which monocytes/macrophages/dendritic cells can influence selected pathways. ROS=reactive oxygen species, IDO=Indoleamine 2,3-dioxygenase 1 Modified from Ref. (3).
F Schematic representation of the homocysteine/methionine pathway and its interplay with choline and hypoxanthine metabolism as well as biosynthesis of GSH. Red and green rectangles denote metabolites significantly upregulated and downregulated, respectively. Hatched red rectangles and hatched green denote metabolites significantly upregulated and downregulated, respectively, but failing to reach log2FC > 0.5. Grey rectangles denote metabolites not significantly changed when comparing patients to healthy controls. Hatched grey rectangles denote metabolites not measured in our dataset. SA methionine=S-adenosylmethionine, SA-homocysteine=S-adenosylhomocysteine, THF=tetrahydrofolic acid, 5-Met-THF=5-methyltetrahydrofolic acid, CDP-Choline=cytidine-5'-diphosphocholine, GSH= glutathione, GSSG= oxidised glutathione.
Adapted from Refs. (4-6)

210x297mm (300 x 300 DPI)